JOURNAL OF PHYSICAL OCEANOGRAPHY VOL. 23, NO. 8 AUGUST 1993

On the Sources of North Atlantic Deep Water*

JAMES LUYTEN, MICHAEL MCCARTNEY, AND HENRY STOMMEL[†]

Woods Hole Oceanographic Institution, Woods Hole, Massachusetts

ROBERT DICKSON AND ED GMITROWICZ

Fisheries Laboratory, Ministry of Agriculture, Fisheries and Food, Lowestoft, United Kingdom

8 January 1992 and 4 December 1992

ABSTRACT

Because the volumetric census of deep and bottom water in the North Atlantic Ocean consists of three isolated linear ridges along which heat and salt flow through the main volumetric mode (and point of intersection), it is possible to deduce the expected ratio of heat flux and ratio of salt fluxes measured in the Denmark Strait overflow off Greenland and in the Antarctic Bottom Water near the equator. The weakly stratified layers of upper North Atlantic Deep Water fall on the nearly linear ridge at temperatures above that of the mode.

There is an incompatibility between observed ratio and deduced ratio. It is predicted that a remeasurement of the flux of Antarctic Bottom Water near the equator will show that the previous determination of 4°N is unrepresentatively low.

1. The S, ϑ volumetric census of the deep and bottom waters of the North Atlantic

The volumetric census of deep waters in the North Atlantic Ocean, given in Plate 1 of Wright and Worthington (1970) and schematically reproduced in Fig. 1, shows a mode centered near potential temperature 2.1°C and salinity 34.91 psu. From the mode, three narrow volumetric ridges radiate in nearly linear fashion as labeled 1, 2, and 3. The volume of the mode is remarkable, with the volume of the four largest volumetric density classes totaling 15.8×10^6 km^3. If this volume were redistributed into a layer of uniform thickness over the (surface) area of the North Atlantic, it would be 429 m thick, or about 11.5% of the average ocean depth. The 12 largest volumetric density classes, indicated in black on the figure, would form a layer 901 m thick, or about 24.2% of the average ocean depth. About one-half of this water is the mode itself; most of the rest lies above the mode forming the high volume linear ridge 3. The waters of mode and the warmer more saline ridge 3 are commonly called North Atlantic Deep Water (NADW). Extending from the mode in the colder/fresher direction is linear ridge 2, which represents the Antarctic Bottom Water flowing northward across the equator from its cold source in the South Atlantic Ocean along the bottom of the western trough, with a branch into the eastern trough through the Vema Fracture Zone at 11°N (McCartney et al. 1991). A few of the largest volume classes are found at the warm end of this ridge adjacent to the mode. Ridge 1 is of much smaller volume and is nearly isohaline extending to near 0°C at its cold source, the Denmark Strait overflow water (DSOW), which flows southward as a fast, steeply banked, thin current along the continental slope of Greenland. The penetration of the cold waters of ridges 1 and 2 into the midlatitude abyss of the North Atlantic Ocean is vividly displayed in the plates of the Worthington and Wright (1970) atlas.

A very good picture of the spatial distribution of the water in these ridges can be obtained by inspection of Plates 2 through 29 of the Worthington and Wright (1970) atlas, which display the depth and salinity of surfaces of constant potential temperature at 0.1° intervals (Fig. 1). The two bottom sources, 1 and 2, can be visualized as two separate plumes of anomalous water that are completely absorbed into the NADW. They are laterally separated and cannot mix with each other. Both the AABW and DSOW yield up all the temperature and salt anomalies that they carry to the overlying NADW through the mode, point 0 (in Fig. 2). Points on the warm ridge, 3, occupy surfaces covering large areas of the North Atlantic, lying above the mode of NADW, point 0. Therefore, this ridge is less like a plume and more like a series of isothermal and isohaline lids, or covers, lying on top of the NADW mode. Through these lids, vertical temperature and salt

* Contribution Number 7943 from the Wood Hole Oceanographic Institution.

[†] Henry Stommel died on 17 January 1992.

Corresponding author address: Dr. James R. Luyten, Woods Hole Oceanographic Institution, Woods Hole, MA 02543-1047.

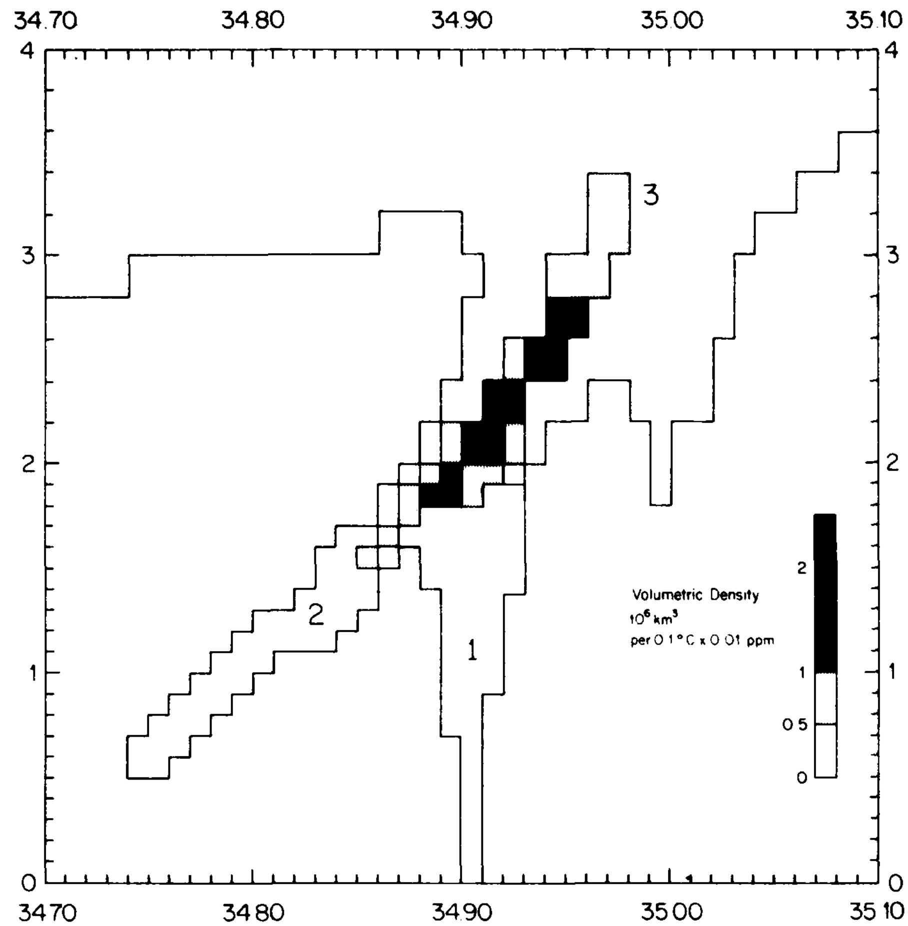

FIG. 1. Simplified version of the bivariate volumetric census of potential temperature and salinity for the North Atlantic Ocean from Wright and Worthington (1970). The ridges 1 and 2 represent bottom water from the Denmark Straits and Antarctic. The high ridge 3 is the large volume of North Atlantic Deep Water.

anomaly fluxes might occur by advection or diffusion at any location, and it is not obvious what the sign and amplitude of the vertical velocity are, because there can be lateral flow across the equator from this stack of lids.

Since the ridges are narrow, the ranges of salinity on any of the potential temperature surfaces is small. This is in marked contrast to the situation at warmer levels above the ridges where the S, ϑ ridges broaden out: for example, at 3.6°C there is a wide range of salinity, and the flux of salinity would depend upon the geographical location of the mass flux. The existence of narrow ridges is therefore an important feature of the part of the S, ϑ diagram (colder than 3°C) that, as we will show, is advantageous in interpreting relations between the fluxes in the three ridges, along which temperature and salt fluxes must be confined.

2. Computation of the slopes λ_i of the ridges

The three ridges are shown schematically in Fig. 2 by lines radiating from the central mode of NADW at S_0, ϑ_0. Although we do not know where realistic "endpoints" lie along the ridges, we need only choose representative points S_i, ϑ_i (i = 1, 2, 3 in Fig. 2) along the ridges to determine their slopes λ_i:

$$\lambda_i = S_i'/\vartheta_i', \tag{1}$$

where the

$$\vartheta_i' = \vartheta_i - \vartheta_0; \quad S_i' = S_i - S_0 \tag{2}$$

are anomalies relative to the S, ϑ of the central mode.

We tried two methods, denoted by A and B, to determine the slopes from the data in Fig. 1. Method A involves determination of the slopes by choosing four

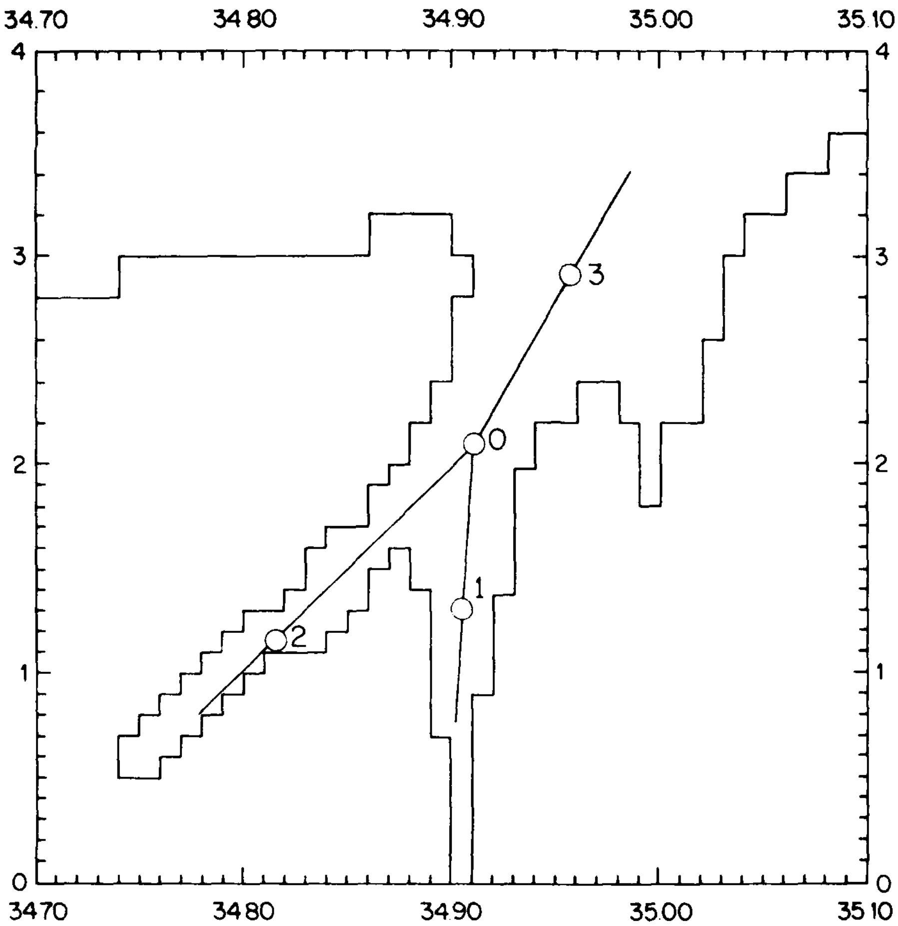

FIG. 2. Schematic configuration of the ridge lines showing their common intersection at point 0. The points 1, 2, and 3 are representative points chosen on the ridges for the purpose of determining the slopes of the lines, as in Table 1 (method A).

representative points on the S, ϑ plane to define the lines. Its weakness is the arbitrariness of choosing the exact location of the mode for NADW, point 0. Method B involves independent fits of straight lines to each of the three ridges, without requiring locating the point 0, and seems to involve less subjectivity and less error. Of course, using method B, one expects that the three lines will have a nearly common intersection near the NADW mode, and we may even interpret this common intersection as representative of NADW.

To proceed with method A, representative points have been taken from Worthington and Wright's plate 1 and entered in Table 1. The points are 0 is the NADW modal peak, 1 lies on the DSOW ridge, 2 on the AABW ridge, and 3 on the overlying warm ridge extending upward toward the base of the thermocline. An "error" range corresponding to the spread of salinity at the given temperature is also given for purposes of tracing errors in subsequent calculations.

To use method B, lines are fitted to each of the three ridges to obtain the slopes λ_i,

$$\text{line 1:} \quad S = 34.905 + 0.0075\vartheta$$

$$\text{line 2:} \quad S = 34.680 + 0.1050\vartheta$$

$$\text{line 3:} \quad S = 34.770 + 0.0650\vartheta.$$

The errors of slope and their computed probable errors are given in Table 2.

There is some small ambiguity in determining the central value assigned to point 0. The highest volumetric density class is centered at 1.95°C, 34.895 psu. The cluster of the four highest volumetric density classes defining the greatest volume mode, and that used for point 0 in method A, is centered at 2.10°C, 34.910 psu. The closest approach to a common intersection of the three lines of method B is at 2.31°C, 34.922 psu. This is quite close to the average of the 12 largest volumetric density classes of Fig. 1, 2.26°C, 34.920 psu. All these points lie on the main ridge of NADW but they are not identical. For subsequent calculations we will use the representative temperature (and salinity) of point 0 as 2.0°C (and 34.90 psu) to define temperature and salinity anomalies.

3. Fluxes of volume, temperature, and salinity on the S, ϑ diagram

Now turn to interpreting the three linear volumetric ridges on the S, ϑ diagram (Fig. 1) as a map upon which to draw the fluxes of volume and of temperature and salinity expressed in terms of anomalies S'_i, ϑ'_i [Eq. (2)] from the temperature and salinity S_0, ϑ_0 of the point 0 where the three ridges meet and the dominant mode occurs. The ridges of Fig. 1 can be thought of as divided into layers defined by incrementally spaced isotherms of temperature anomaly ϑ'_j, where j is an index defined negative for temperatures colder than ϑ_0 and thus corresponds to the cold waters of ridges 1 and 2 with negative temperature anomalies. The mode itself corresponds to $j = 0$, is by definition a temperature anomaly of zero, and is included as the cold end of the high volume ridge 3, which thus has $j \geq 0$, with temperature anomalies ≥ 0. In physical space it is visualized that cross-equatorial flow supplies ridge 2 with AABW as a volume transport $U_{2,j}$ in the classes $j < 0$, while the Denmark Strait overflow supplies DSOW from the north to ridge 1, as a volume transport $U_{1,j}$ in the classes $j < 0$. In the north we assume that there is no exchange with the Norwegian Sea involving waters warmer than ϑ_0 associated with ridge 3, $j \geq 0$, based on the thermal structure along the Iceland–Scotland Ridge (Mann 1969; Saunders 1990; Tait et al. 1967). Volume transports $U_{3,j}$ across the equator are permitted for the warmer classes $j \geq 0$; this is the export of NADW to the rest of the World Ocean.

TABLE 1. Method A: values of representative points and computed fluxes.

Point i	ϑ_{pot} (°C)	S (psu)	Error	ϑ'_i	S'_i
0	2.10	34.91	+.01		
1	1.35	34.905	+.005	.75	.005
2	1.15	34.815	+.005	.95	.095
3	2.9	34.959	+.005	+.80	+.049
		$\frac{\Theta_2}{\Theta_1}$ 1.50 + .5			
		$\frac{\Theta_3}{\Theta_1}$ 2.50 + .5			

TABLE 2. Method B: values of fitted slopes and computed fluxes.

Line i	λ Slope $\frac{dS}{d\vartheta}$ (psu °C)	Error estimate
1	+.0075	+.005
2	+.1050	+.005
3	+.0650	+.005
	$\frac{\Theta_2}{\Theta_1}$ 1.50 + .17	
	$\frac{\Theta_3}{\Theta_1}$ +2.50 + .17	

Closest approach of lines at 2.31°C, 34.922° psu.

This deep circulation system can be visualized in plan view through the plates of the Worthington and Wright (1970) atlas, which show the progressive penetration of the AABW and DSOW tongues to midlatitude. Figure 3 attempts an orthogonal view with a schematic rendition of this layered system of water masses in a meridional plane representing the zonally averaged vertical and meridional flow. We have indicated midlatitude physical contact between ridges 1 and 2 for a single layer, $j = -1$, as an example. The Worthington and Wright (1970) atlas suggests that the contact occurs at a temperature between 1.8° and 1.9°C southeast of Newfoundland. In addition to the cross-equatorial and Norwegian Sea volume transports $U_{i,j}$, volume transports between layers are indicated

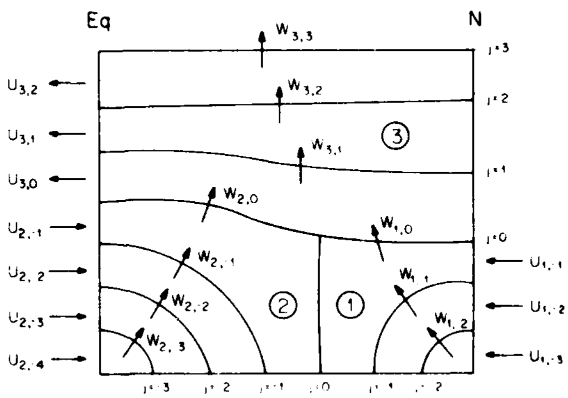

FIG. 3. Schematic vertical meridional section of the deep North Atlantic showing the spatial relation of the three masses of water in the ridges. The contours labeled j are of potential temperature anomaly. At $j = 0$ the potential temperature anomaly is zero, corresponding to the temperature at point 0 in Fig. 2. Mass fluxes $U_{i,j}$, $W_{i,j}$, defined by the figure, have the index i to indicate the number of the ridge and index j to indicate the isothermal surface with which they are associated.

as $W_{i,j}$. These are required by continuity by the observed disappearance of colder isotherms at midlatitudes (Worthington and Wright 1970), the net lateral inflow to a layer has no exit except across its upper bounding isotherm. We note that there is diffusion explicit in this schematic: an inflow $U_{i,j}$ to a layer occurs at the average temperature of its bounding isotherms, while the outflow $W_{i,j}$ occurs at the upper bounding isotherm temperature. For example, for $j < 0$ with the expected $U_{i,j} > 0$, the resulting $W_{i,j}$ increases with the index j, and a downward diffusion of heat is required for steady state.

Upon reflection, the reader will recognize that generally there must also be a diffusive component of temperature flux across each isothermal surface in each ridge, otherwise the temperature field could not be in a steady state. To see this clearly one needs only to note that, for example, in ridge 2 there is a net negative ϑ' advected into it from the south by the $U_{2,j}$ and yet at $j = 0$, even though $W_{2,0} > 0$, the $\vartheta'_0 = 0$ so there can be no negative ϑ' advected out of this ridge's top through the branch point 0. Therefore, at $j = 0$ the fluxes of temperature anomaly in all three ridges must be entirely diffusive. They may be denoted at $j = 0$ by Θ_i. The Θ fluxes without a j suffix are taken to have $j = 0$. Two of these temperature fluxes are known:

$$\Theta_1 = \sum_{j=J}^{-1} U_{1,j}(\vartheta'_j + \vartheta'_{j+1})/2$$

$$\Theta_2 = \sum_{j=J}^{-1} U_{2,j}(\vartheta'_j + \vartheta'_{j+1})/2. \tag{3}$$

These expressions have a paradoxical appearance. The Θ_i are diffusive, whereas the right-hand side is purely advective. The third flux Θ_3 is known by continuity of temperature flux through the branch point 0:

$$\Theta_3 = \Theta_1 + \Theta_2. \tag{4}$$

We can visualize the flux of volume and temperature anomaly ϑ' along ridge 2 from its cold end to where it joins the branch point 0 in the following manner: as ϑ' increases, volume flux increases and negative flux of temperature increases. At the branch point 0, where $\vartheta' = 0$, the entire transport of the negative temperature ϑ' becomes diffusive by definition. The same can be said of ridge 1.

Because of the linear form of the ridges, the assignment of discrete salinity values to each value of j differs from those of the temperature in each ridge by only the constant factor λ_i. If the turbulence that causes the diffusive component of fluxes does not differentiate between temperature and salinity, then the conservation equations for salt differ only by the factor λ_i from those for temperature. Thus, if the flux of salinity for each of the three ridges is denoted by $\mathcal{S}_i$, we can write

$$\mathcal{S}_i = \lambda_i\Theta_i, \tag{5}$$

and then by conservation of salt flux across the branch point

$$\mathcal{S}_3 = \mathcal{S}_1 + \mathcal{S}_2 = \lambda_1\Theta_1 + \lambda_2\Theta_2 \tag{6}$$

or

$$\lambda_3\Theta_3 = \lambda_1\Theta_1 + \lambda_2\Theta_2. \tag{7}$$

There are therefore two homogeneous equations, (4) and (7), for the three Θ_i, and consequently we can determine various ratios between the Θ_i in terms of the measured slopes:

$$\frac{\Theta_2}{\Theta_1} = \frac{\lambda_3 - \lambda_1}{\lambda_2 - \lambda_3}, \quad \frac{\Theta_3}{\Theta_1} = \frac{\lambda_1 - \lambda_2}{\lambda_3 - \lambda_2}. \tag{8}$$

Values of these ratios computed from the slopes are given in Tables 1 and 2 along with estimated error.

The ratio Θ_2/Θ_1 is of particular interest because it can be used to check against the available measurements of fluxes into the North Atlantic along ridges 1 and 2: the Denmark Strait overflow water (DSOW) and the Antarctic Bottom Water (AABW). A summary of the estimates of these directly observed fluxes is given in the next section, and the comparison is made.

Now we turn our attention to consideration of ridge 3 along which the populous volumetric classes of NADW are arrayed. This ridge extends from 2.0°C potential temperature to 2.9°C (or $\vartheta' = 0$ to 0.9°) before it intersects other water masses from the Faeroe–Iceland Ridge, Labrador Sea, and saline water masses at the base of the main thermocline. In the absence of directly measured volume fluxes of either U_{3j} or W_{3j}, we cannot distinguish between the diapycnal mass flux, W_{3j}, upward into the thermocline and the isopycnal advective flux, U_{3j}, across the equatorial boundary of the model.

4. Measurements of fluxes in waters described by ridges 1 and 2

At this point we introduce another type of data: measurements of advective fluxes entering ridges 1 and 2 at the northern and southern boundaries of the total portion of the North Atlantic Ocean covered by the S, ϑ diagram in Fig. 1. These provide numerical estimates of W_1, W_2, Θ_1, Θ_2 at the branch point 0. We will then be able to see whether the ratio Θ_2/Θ_1 computed by Eq. (8) from the slopes of the ridges agrees with the ratio observed. This will give us some indication about which of the direct measurements may be unrepresentative of long-term means.

To be useful the quantities Θ_1, Θ_2 (and possibly $\mathcal{S}_1$, $\mathcal{S}_2$ for checking) need to be measured at sections as close to the origin of the plumes as possible, at the northern and southern latitudes of the volume described in the census. These measured integrated fluxes of bottom waters (on ridges 1 and 2) across the sections are regarded as purely advective—no diffusive process is considered. Because the thermal anomalies ϑ_1', ϑ_2' and salinity anomalies S_1', S_2' are all negative, the integrated fluxes Θ_1, Θ_2, $\mathcal{S}_1$, $\mathcal{S}_2$ are also all negative. Thus, the volume fluxes into the North Atlantic along ridges 1 and 2 both carry coldness and freshness to the NADW.

a. Ridge 1

Ross (1984) measured the volume fluxes of water of different temperatures in the DSOW along the continental slope of Greenland south of the Denmark Strait using current meters and hydrographic stations for geostrophic current calculations. An estimate of $\Theta_1 = -4.6$°C Sv (relative to 2°C) was made graphically from Ross's Fig. 6 (Sv ≡ 10^6 m^3 s^{-1}).

The section occupied was close to the sill, and it seems that some of the cold water on the section may actually be too fresh to sink to greater depths, so this value of Θ_1 may be too large for heat flux into the deep western boundary current off Greenland. Dickson et al. (1990) have maintained an array of instruments off Angmagsalik across the current where it is deeper. An estimate of Θ_1 from the current meters and a hydrographic section yields Θ_1 = 2.46°C Sv, as shown in Table 3.

b. Ridge 2

Whitehead and Worthington (*1982, hereafter WW*) made detailed enumerations of the heat flux carried northward by the AABW at 4°N by two methods: current meter–measured currents and temperatures and geostrophic calculations from hydrographic data. Using columns 3 and 9 of their Table 3 we obtain Θ_2 = 0.48°C Sv from the current meter data and Θ_2 = 1.45°C Sv from the geostrophic calculations. Both of these estimates may be too low, and a detailed reexamination is given by McCartney (1993a). The baroclinic signature of the northward flow of AABW is eastward-rising isotherms, and at 4°N, these fill the basin (Fig. 4). The two current meter moorings used

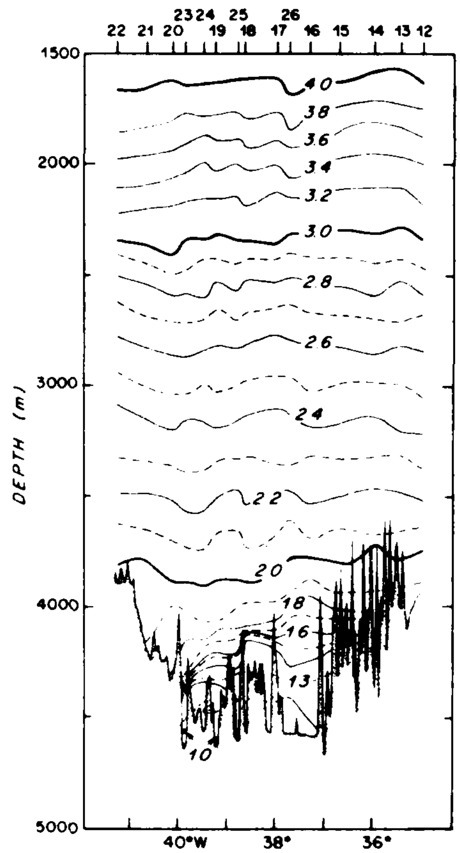

FIG. 4. A recontouring of the potential temperature distribution of the 4°N section of Whitehead and Worthington (1982) data as proposed by McCartney (1993a) to show more of the deep water.

were located in the west and sampled at best only the western third of the flow. The abyssal basin is about 350 km wide at 4°N; WW attributed their moored measurements to a width of 84 km and implicitly assumed zero transport for the rest of the passage—about 370 km! Their eastern mooring was placed atop a shoal and sampled only as cold as 1.27°C in a region where coldest temperatures are 0.98°C (at about 250 m deeper than this shoal). Whitehead and Worthington attributed 70% of their total AABW transport to this mooring, which, leaving aside the issue of the width that mooring can be attributed to, would appear to be biased warm. The other mooring, with 30% of the AABW transport, showed a pronounced decrease in northward speed towards the bottom, about 62%. This shear disagreed with the northward geostrophic shear from bracketing hydrographic stations, which show northward speed increasing towards the bottom. The simplest explanation is that the mooring represents the flow from a narrower region than the distance between

TABLE 3. Θ_1 computed for differing ranges of deep water (from Dickson et al.)

θ range (°C)	$(\theta_i - 2) \times$ transport (°C Sv)	Transport (Sv)
<1	0.38	0.34
<1.5	2.11	2.64
<2.0	2.46	4.06
<2.5	1.86	6.48
<3.0	+0.71	9.90
<3.25	+1.63	10.72

the hydrographic stations sampled. In addition, while the mooring showed northward speeds decreasing near the bottom about 62%, the vector velocity magnitude decreased here only 35% while veering right about 52°, suggesting topographic steering of the deepest flow.

We regard the current meter results as underestimates of the total volume transport and as warm biased as to their heat transport. For the current meter data one factor in the underestimation of heat transport is the underestimation of volume transport, due to the restriction to the western fourth of the basin and the measured decline of northward speed towards the bottom. The other compounding factor is the warm bias in the estimate of the temperature being transported: at the western mooring due principally to the decrease in speed with depth, and at the eastern mooring due to the mooring sampling only the warmer levels of the AABW. For both moorings the coldest waters in the attributed areas were assumed not to be moving. The effects of the speed decrease with depth would be considerably reduced if vector velocity were used rather than northward speed, since it is the total flow of AABW along its stream tube that is important, not the local orientation of that tube. As noted above, the vector magnitude at the eastern mooring did not decrease nearly so much with depth as the northern component did.

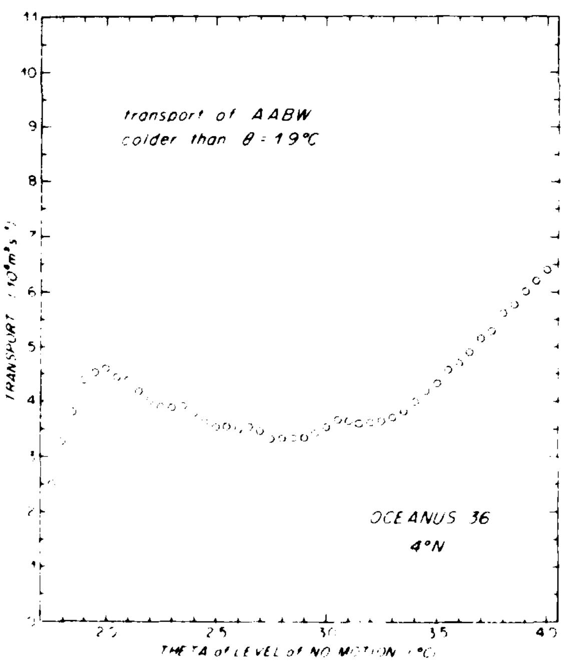

FIG. 5. Recalculation of geostrophic volume transport across 4°N section (Fig. 4) as a function of the potential temperature isotherm chosen as the level of no motion.

Figure 5 shows the results of a recent recalculation of the geostrophic volume transport for the WW 4°N section (Fig. 4), focusing on the effect of the selected level of no motion on the total volume transport. Here WW estimated 1.98 Sv using a level of no motion of 1.9°C; the new calculation gives 4.42 Sv for that same level. Reexamination of WW's original calculation records shows a computational error at the eastern station pair 16–15 that contributes 0.96 Sv to the difference. Our new calculation does not use this station pair at all because it has topography intervening that completely penetrates the AABW. Various other things contribute to the remaining difference of 1.55 Sv principally involving differences in estimation of transport in the bottom triangles of hydrographic station pairs. These are discussed by McCartney (1993a). For the present purpose we use the corrected WW transport of 2.94 Sv as a lower bound and simply scale their heat transport upward by the factor 2.94/1.98 to obtain a lower bound on the heat transport of −2.15°C Sv. For a second estimate, the maximum AABW transport from Fig. 5 is used that occurs for a deep level of no motion at 2.00°C, 4.60 Sv, which carries a heat transport of −3.11°C Sv. Finally, for an estimate of an upper bound, we choose a level of no motion of 3.7°C giving a transport of AABW of 5.13 Sv carrying a heat transport of −4.00°C Sv. Such a shallow level of no motion gives a more gyrelike aspect to the deep water circulation as discussed by McCartney (1993b).

5. Computation of $\mathcal{S}_3/\Theta_3$

In Table 4, the values of $\mathcal{S}_3/\Theta_3$ computed from various values of Θ_1 and Θ_2—according to (8)—are shown. These are to be compared to $\lambda_3 = 0.065$ psu °C^{-1} as determined from the S, ϑ diagram. All values of $\mathcal{S}_3/\Theta_3$ computed from published temperature anomaly fluxes along ridges 1 and 2 are lower than the observed λ_3, and we conclude that one or more of the measured fluxes is not representative of the long-term mean. As discussed in section 2, we suspect that the published estimates for Θ_2 are too small. Our conjecture that the long-term mean Θ_2 is in the range $-4.0 < \Theta_2 < -3.1$°C Sv to yield a value of $\mathcal{S}_3/\Theta_3$ consistent with λ_3. This larger value of Θ_2 could be confirmed by further direct observations of the fluxes in ridge 2.

6. Estimate of the vertical diffusivity at $\vartheta = 2.0$°C

Our conjecture of the flux of potential temperature anomaly along ridge 2, together with the measured flux along ridge 1, yields a total flux of potential temperature anomaly relative to $\vartheta = 2.0$ of -5.9°C Sv. By definition, this is a diffusive flux at point 0 (-2°C), so that we can estimate a thermal diffusion coefficient:

TABLE 4. Values of flux ratio K/Θ_3 computed from Eq. (8) [illegible] compared with [illegible] 0.065. The Θ and Θ are in [illegible] Sv.

	Θ		
Θ_2	Dickson et al. 2.46	Ross 4.6	Scaled Ross 3.1
WH (current meter) 0.48	0.023	0.017	0.021
WH (corrected geostrophic) 1.45	0.044	0.031	0.039
Our new (deep reference 2°C) 3.11	0.062	0.047	0.056
Our new (middepth reference 3.2°C) 4.00	0.068	0.053	0.062

$$K = \frac{\Theta_3}{-A(\partial\vartheta/\partial z)_{\vartheta=2^\circ\mathrm{C}}},$$

where A is the area of the 2° potential temperature surface. We estimate A to be 14×10^6 km^2 and $(\partial\vartheta/\partial z)_{\vartheta=2^\circ\mathrm{C}} = 10^{-3}$ °C/m, giving $K = 4$ cm^2 s^{-1}.

Acknowledgments. We wish to thank Dr. Peter Saunders of the Institute of Oceanographic Sciences, United Kingdom, for detecting a serious blunder in the first version of this note. Dr. R. X. Huang offered important criticism and suggestions. J. Luyten is supported by Office of Naval Research Grants N00014-90-J-1508 and N00014-90-J-1425. M. McCartney is supported by National Science Foundation Grant OCE86-14486, and H. Stommel by Grant OCE89-13128.

REFERENCES

Dickson, R. R., E. M. Gmitrowicz, and A. J. Watson, 1990: Deep water renewal in the northern North Atlantic. *Nature*, **344**, 848–850.

Mann, C. R., 1969: Temperature and salinity characteristics of the Denmark Strait overflow. *Deep-Sea Res.*, **16** (Suppl.), 125–137.

McCartney, M. S., 1993a: The transport of Antarctic Bottom Water at 4°N in the western basin of the North Atlantic Ocean. *J. Geophys. Res.*, in press.

——, 1993b: The crossing of the equator by the deep western boundary current in the western Atlantic Ocean. *J. Phys. Oceanogr.*, **23**, 1953–1974.

——, S. L. Bennett, and M. E. Woodgate-Jones, 1991: Eastward flow through the Mid-Atlantic Ridge at 11°N and its influence on the abyss of the eastern basin. *J. Phys. Oceanogr.*, **21**, 1089–1121.

Ross, C. K., 1984: Temperature–salinity characteristics of the "overflow" water in Denmark Strait during "OVERFLOW '73." *Rapp. Proc. V. Reun. Cons. Perm. Int. Explor. Mer*, **185**, 111–119.

Saunders, P. M., 1990: Cold outflow from the Faroe Bank Channel. *J. Phys. Oceanogr.*, **20**, 29–43.

Tait, J. B., A. J. Lee, U. Stefansson, and F. Herman, 1967: Temperature and salinity distributions and water masses of the region. *The Iceland–Faroe Ridge International (ICES) "Overflow" Expedition, May–June 1960. An Investigation of Cold, Deep Water Overspill into the Northeastern Atlantic Ocean*, J. B. Tait, Ed., *Rapp. Proc. V. Reun. Cons. Perm. Int. Explor. Mer*, **157**, 38–149.

Whitehead, J. A., Jr., and L. V. Worthington, 1982: The flux and mixing rates of Antarctic bottom water within the North Atlantic. *J. Geophys. Res.*, **87**, 7903–7924.

Worthington, L. V., and W. R. Wright, 1970: North Atlantic Ocean atlas of potential temperature and salinity in the deep water including temperature, salinity, and oxygen profiles from the Erika Dan cruise of 1962. *Woods Hole Oceanographic Institution Atlas Series*, **2**, 24 pp. and 58 plates.

Wright, W. R., and L. V. Worthington, 1970: The water masses of the North Atlantic Ocean—A volumetric census of temperature and salinity. *Serial Atlas of the Marine Environment*, Folio 19, Amer. Geogr. Soc., 8 pp. and 7 plates.

REPORT DOCUMENTATION PAGE

Form Approved
OMB No. 0704-0188

1. AGENCY USE ONLY *(Leave blank)*

2. REPORT DATE
9/93

3. REPORT TYPE AND DATES COVERED
TECHNICAL

4. TITLE AND SUBTITLE
ON THE SOURCES OF THE NORTH ATLANTIC DEEP WATER

5. FUNDING NUMBERS
ONR N00014-90-J-1508
ONR N00014-90-J-1425
NSF OCE86-14486
NSF OCE89-13128

6. AUTHOR(S)
JAMES LUYTEN, MICHAEL MCCARTNEY AND HENRY STOMMEL

7. PERFORMING ORGANIZATION NAME(S) AND ADDRESS(ES)
WOODS HOLE OCEANOGRAPHIC INSTITUTION
WOODS HOLE, MA 02543

8. PERFORMING ORGANIZATION REPORT NUMBER
WHOI CONTR. 7943

9. SPONSORING/MONITORING AGENCY NAME(S) AND ADDRESS(ES)
OFFICE OF NAVAL RESEARCH
ENVIRONMENTAL SCIENCES DIRECTORATE
ARLINGTON, VA 22217-5660

10. SPONSORING/MONITORING AGENCY REPORT NUMBER

11. SUPPLEMENTARY NOTES
In citing this report in a bibliography, the reference given should be:
JOURNAL OF PHYSICAL OCEANOGRAPHY 23(8):1885-1892, 1993

12a. DISTRIBUTION/AVAILABILITY STATEMENT
APPROVED FOR PUBLIC RELEASE:
DISTRIBUTION UNLIMITED

12b. DISTRIBUTION CODE

13. ABSTRACT *(Maximum 200 words)*

Because the volumetric census of deep and bottom water in the North Atlantic Ocean consists of three isolated linear ridges along which heat and salt flow through the main volumetric mode (and point of intersection), it is possible to deduce the expected ratio of heat flux and ratio of salt fluxes measured in the Denmark Strait overflow off Greenland and in the Antarctic Bottom Water near the equator. The weakly stratified layers of upper North Atlantic Deep Water fall on the nearly linear ridge at temperatures above that of the mode.

There is an incompatibility between observed ratio and deduced ratio. It is predicted that a remeasurement of the flux of Antarctic Bottom Water near the equator will show that the previous determination of 4°N is unrepresentatively low.

14. SUBJECT TERMS
1) NORTH ATLANTIC DEEP WATER
2) ANTARCTIC BOTTOM WATER
3) ABYSSAL CIRCULATION

15. NUMBER OF PAGES
8

16. PRICE CODE

17. SECURITY CLASSIFICATION OF REPORT	18. SECURITY CLASSIFICATION OF THIS PAGE	19. SECURITY CLASSIFICATION OF ABSTRACT	20. LIMITATION OF ABSTRACT
UNCLASSIFIED	UNCLASSIFIED	UNCLASSIFIED	